

Spin Hall magnetoresistance in paramagnetic NdGaO₃

V. Eswara Phanindra,^{1,*} A. Das,¹ J. J. L. van Rijn,¹ S. Chen,¹ B. J. van Wees,¹ and T. Banerjee^{1,†}

¹University of Groningen, Zernike Institute for Advanced Materials, 9747 AG Groningen, The Netherlands

(Dated: January 24, 2022)

In recent years, spin Hall magnetoresistance (SMR) has emerged as an efficient way to probe the spontaneous magnetization state in ordered magnetic systems, by electrical current. Less known is its versatility as a probe of materials that do not possess spontaneous magnetization such as in paramagnets. In this work, SMR is used to probe paramagnetic NdGaO₃ (NGO), a rare earth oxide, possessing a sizable spin orbit interaction (L=6). NGO has not been investigated earlier for its efficiency in propagating spins. We have performed extensive temperature and angle dependent-magnetoresistance (ADMR) studies along dissimilar crystallographic axes in NGO, using platinum (Pt) as spin injector and detector and utilizing (inverse) spin Hall effect. We find a close correlation between the temperature dependence of the ADMR response with magnetization in NGO and a linear current bias dependence of the ADMR amplitudes. These are characteristics of SMR effect in Pt/NGO, arising from the torque acting on localized moments in NGO and considering crystal field induced intermultiplet transitions with temperature. Control experiments on Pt/SrTiO₃ and Pt/SiO₂ devices were also carried out in order to validate the observed SMR response in Pt/NGO bilayer and to rule out magnetoresistive contributions from Pt.

I. INTRODUCTION

Spin Hall magnetoresistance (SMR) is commonly used as an efficient means to electrically access the magnetic order of an underlying magnetic material, using normal metals (NM) such as Pt with large spin orbit coupling (SOC)¹⁻⁴. SMR is primarily a resistance modulation effect, arising from a collective interaction due to the spin Hall effect, spin-transfer torque, and inverse spin Hall effect at the (anti-)ferromagnetic insulator FMI or AFI/NM interface^{2,5-11}. Earlier spin transport and SMR studies focused mostly on ordered magnetic systems, exhibiting spontaneous magnetization, whereas studies on paramagnetic insulators (PM-I) are scarce¹²⁻¹⁵. However, study of SMR in paramagnets, materials that are confined to a passive role, for instance as spacer layers, in spin valves¹⁶ might be useful for designing new spintronic devices. In order to realise and establish paramagnet-based spintronics, thorough characterization of these materials by spin transport based approaches such as SMR, is thus essential. Further, SMR measurements on PMs provide information about interfacial parameters such as spin conductance, which in turn govern the interfacial exchange interaction (J_{exc}) between the conduction electrons in the Pt layer and localized moments of the PM layer. Experimental evaluation of these parameters will be important in advancing the microscopic theory of SMR¹⁷.

In this regard, we experimentally demonstrate the SMR effect in a new paramagnetic insulator, NdGaO₃ (NGO). NGO, has a good lattice match for the growth of high quality and strained complex oxide thin films such as rare earth manganites, high T_C superconductors, etc¹⁸. NGO exhibits an orthorhombic distorted perovskite structure with lattice constants denoted in orthorhombic notation as $a = 5.43 \text{ \AA}$, $b = 5.70 \text{ \AA}$, and $c = 7.71 \text{ \AA}$ belonging to the Pbnm space group¹⁹, while in pseudo cubic notation the lattice constant of NGO corresponds

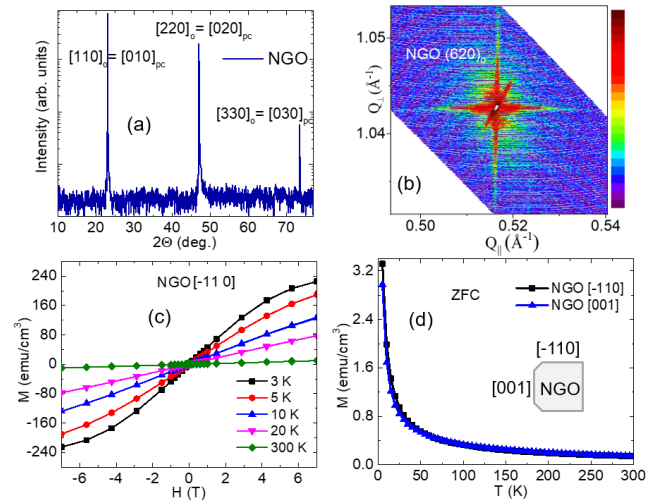


FIG. 1. (a, b). $\theta - 2\theta$ scan and reciprocal space map (RSM) of (6 2 0) asymmetric reflection of NdGaO₃ (110)_o single crystalline substrate. Fig. 1(c) Magnetization (M) vs applied magnetic field (H) loops measured at different temperatures. Fig. 1(d) Magnetization (M) vs temperature (T) plots measured at an applied field of $H = 1000 \text{ Oe}$ along two in-plane orthogonal (i.e. [001]_o and [-110]_o) crystallographic axes.

to about 3.86 \AA . For this study, we chose [110]_o oriented NGO along the out-of-plane direction, with the in-plane edges correspond to [-110]_o and [001]_o directions. Although NGO is a PM insulator, at temperatures below 1 K, it orders into an antiferromagnetic (AFM) phase, with dissimilar exchange (J_{ex}) interactions along the out-of-plane and in-plane directions¹⁸. In DyScO₃ (PM-I), analogous to NGO, it was shown that short range correlations can favor the manifestation of spin Seebeck signals (SSE)²⁰ at very low temperatures. Recent studies on PM-Gd₃Ga₅O₁₂ (GGG), using SMR, demonstrate efficient spin current transport persisting

up to ~ 100 K and ascribed to the dipolar exchange interactions between the localized spins¹². A theoretical study on SSE suggests that the paramagnetic-SSE signal is proportional to external magnetic field times the spin susceptibility of the magnet (or field-induced magnetization in PM-I)²¹.

In this manuscript we perform SMR studies in paramagnetic-NGO single crystalline substrates and observe spin transport persisting up to ~ 250 K, far beyond the T_N . The persistence of the observed SMR signals over a large temperature range suggest the inadequacy of the earlier explanations such as, dipolar exchange interactions¹² and short-range correlations, as applied for GGG²⁰, to explain our observations. To understand our findings, we recall the magnetic and crystal field induced intermultiplet transitions with temperature of the Nd^{3+} ions, as discussed in earlier studies on NGO²²⁻²⁴. We propose the self-interactions between the correlated 4f orbitals due to crystal field effects, J mixing between the multiplets, the temperature driven electronic excitations between crystal field split levels and spin flip scattering across HM/PI to explain our observations^{23,25}. This is distinctly different from those used to explain SMR effects in GGG/Pt system^{12,20}. Our observation of SMR upto high temperatures (~ 250 K) in PM-NGO is unique and implies that long-range magnetic ordering might not be an essential pre-requisite for efficient spin transport in paramagnets. Our work not only enriches material perspectives but triggers new considerations to the theoretical framework of SMR while encompassing material systems that do not exhibit spontaneous magnetic ordering.

II. STRUCTURAL AND MAGNETIC CHARACTERIZATION

Crystal structure measurements such as θ - 2θ scans and reciprocal space maps(RSM's) were performed on a NGO single crystalline substrate using PANalytical x-ray diffractometer equipped with a four-axis cradle (Cu k_α radiation, $\lambda = 1.54$ Å) to substantiate the phase purity and its crystallographic directions [Fig. 1(a)]. θ - 2θ scan display only multiples of $[110]_o$ peaks along the out-of-plane direction, complemented by RSM scan [Fig. 1(b)], which depicts high substrate crystalline quality devoid of any twin domains or additional impurity phases. Similarly AFM micro-graphs within the scanning area of $5 \times 5 \mu\text{m}^2$ indicate smooth surface morphology of NGO with a surface roughness of 101 pm [Fig. S1]. Temperature (5-300 K) and magnetic field dependent (upto 7 T) magnetization curves of NGO substrate were measured by SQUID magnetometer (Quantum Design).

Fig. 1(c) shows the Magnetization(M) vs applied magnetic field (H) loops measured at different temperatures. Fig. 1(d) depicts the magnetization vs temperature (M-T) curves recorded in zero field cooled (ZFC) and field cooled (FC) modes from 300 K to 5 K at an applied field of 1 kOe along two in-plane orthogonal (

$[001]_o$ and $[-110]_o$) crystallographic axes for NGO sample. Both the M vs H and M vs T plots of the NGO substrate indicate a typical paramagnetic behavior, over a wide temperature range. At low temperatures, the difference of magnetization acquired along in-plane orthogonal (i.e. $[001]_o$ and $[-110]_o$) axes though subtle, is clearly visible, indicating $[-110]_o$ direction as the relatively easy axis and $[001]_o$ direction as the hard axis respectively. This difference is ascribed to the magneto-crystalline anisotropy in NGO²⁶.

III. MAGNETOTRANSPORT MEASUREMENTS

For magneto transport measurements, 11 nm thick-Pt based Hall bar devices (dimensions: width $w = 30 \mu\text{m}$, length $l = 3000 \mu\text{m}$) on NGO single crystalline substrate (as shown in Figs. 2, S2) are patterned and fabricated by photo-lithography followed by sputtering techniques respectively. An optical image of the Pt Hall bar device fabricated on top of NGO single crystalline substrate along two (i.e. $[001]_o$ and $[-110]_o$) crystallographic directions is presented in the supplementary Fig. S2. All the angle dependent magneto-resistance (ADMR) measurements are performed on physical property measurement system (PPMS, Quantum Design) from 5 K to 300 K and upto 7 T magnetic field strength. An alternating sinusoidal charge current was applied to the Pt Hall bar and the voltage response across the longitudinal and transverse directions were simultaneously measured as a first harmonic response $V_{xx}^{1\omega}$ and $V_{xy}^{1\omega}$ at phase = 0° by two lock-in amplifiers. Typically, the ADMR measurements were performed with an AC current of amplitude 3 mA, at a reference frequency of 7.77 Hz and a time constant of 3 seconds was employed while rotating the sample in the in-plane(x-y) and out-of-plane(x-z), (y-z) configurations. Fig. 2(top panel) shows the schematic illustration of the angle dependent measurement geometry and the corresponding sample rotation along the x-y (α), y-z (β) and x-z (γ) directions with respect to the applied magnetic field direction. The electrical current density (J_c) along the x direction in Pt layer induces spin accumulation (σ) along y and spin current density (J_s) along z-direction (due to spin Hall effect), thus mutually orthogonal to each other and related as¹ The spin current density (J_s) induced in the Pt layer exerts a torque on the field induced net magnetization (M) vector of the underlying NGO substrate. Depending on the relative orientation between M and σ , reflection or absorption of spin current occurs at the Pt/NGO interface which in turn causes the modulation of spin dependent magneto-resistance. Thus the resistance maximizes when $M \perp \sigma$ while minimal resistance change occurs for the parallel case (i.e. $M // \sigma$)³. The typical longitudinal and transverse SMR response at the Pt/NGO interface can be expressed as follows^{1,2,8}:

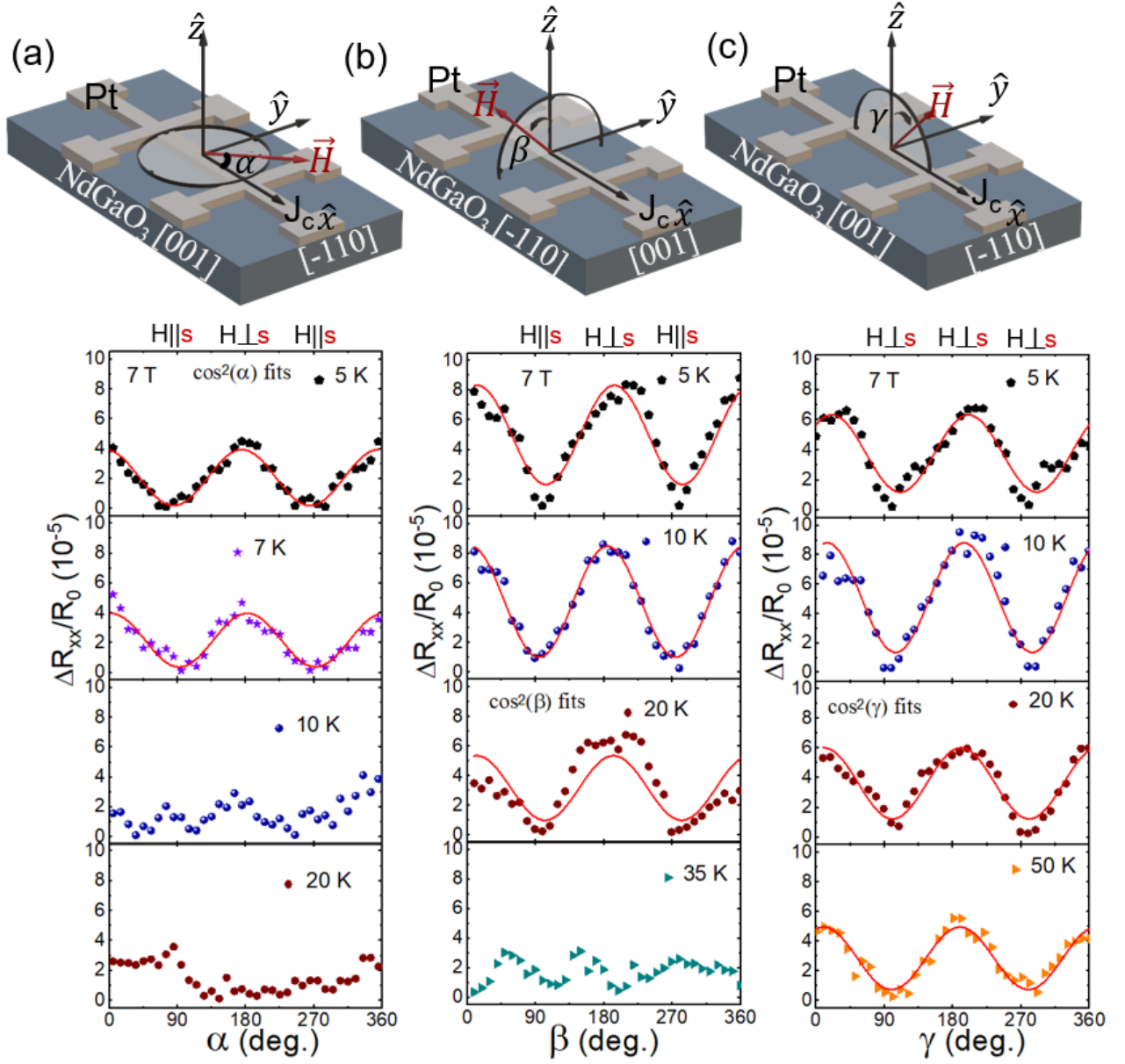


FIG. 2. Schematic illustration of the Hall bar geometry (top panel) and angle dependent magneto-resistance (ADMR) curves (bottom panels) in the longitudinal contacts ($\Delta R_{xx}/R_o$) in Pt (11 nm)/NdGaO₃ (110)_o, for selected temperatures where ADMR signals show noticeable changes. The ADMR signals are measured at different temperatures, and by rotating the sample with respect to a constant magnetic field of 7 T along (a) x-y (α -scan), (b) y-z (β -scan) and (c) x-z (γ -scan) planes. Here s, J_c , H represents the corresponding spin accumulation, charge current and magnetic field directions respectively. The red solid lines are fits to experimental data with a $\cos^2(\alpha)$ function.

$$\frac{\Delta R_{xx}}{R_o} = \frac{\Delta \rho_{xx}}{\rho_o} \langle 1 - m_y^2 \rangle \propto \cos^2(\alpha) \quad (1)$$

$$\frac{l}{w} \frac{\Delta R_{xy}}{R_o} = 2 \frac{\Delta \rho_{xy}}{\rho_o} \langle m_x m_y \rangle \propto \sin(2\alpha) \quad (2)$$

where $\Delta R_{xx}/R_o$ and $\Delta R_{xy}/R_o$ are the longitudinal and transverse SMR amplitude variations respectively.

Similarly, m_x , m_y and m_z denotes the projection of the net magnetization along the three orthogonal axes. R_o is the Drude resistance, $l = 325 \mu\text{m}$ is the distance between the longitudinal contacts, $w = 30 \mu\text{m}$ is the width of Hall bar respectively. Fig. 2(a, b, c) shows the ADMR curves in Pt/NGO sample along three directions as shown in the schematic illustration at low temperatures for 7 T field. The longitudinal magnetoresistance variations shown for Pt/NGO, follows a $\cos^2(\alpha)$ variation implying positive SMR response, consistent with the equations (1,2), as

usually observed in ferro-, ferri-, and para-magnets^{2,3,14}.

Additionally, Fig. 2(c) depicts resistance modulation in the γ scan at low temperatures, which can arise due to weak antilocalization (WAL)²⁷, and is usually observed in heavy metals at low temperatures and high magnetic fields. Moreover for both β and γ scans (out-of-plane scans, Fig. 2(b, c)) the magnitude of the resistance modulation is larger than the in-plane α scan and typical of WAL. To confirm this and to decouple it from SMR, we have performed a thorough and systematic field dependent magnetoresistance (FDMR) measurements on Pt/NGO, Pt/SiO₂ and Pt on single crystalline cubic SrTiO₃ devices, along three orthogonal directions as shown in Fig. 3. Along the out-of-plane direction (Fig. 3), all the devices exhibit qualitatively similar field dependent signature of WAL (independent of the underlying substrate), implying the intrinsic contribution of Pt and consistent with previous reports^{27,28}. Further, the FDMR response (Fig. 3) measured along the in-plane directions for both the Pt/SiO₂ and Pt/SrTiO₃ devices show a quadratic MR response characteristic of a positive-ordinary MR reiterating the intrinsic contribution of the Pt layer^{27,28}. On the other hand the MR response for the Pt/NGO device, exhibits deviation from the quadratic behavior, implying a minor contribution due to SMR. Thus the FDMR measurements shown in Fig. 3, performed on control devices with different para- and dia-magnetic substrates, effectively explains our observed ADMR signals in α , β and γ scans.

Other contributions, such as Hanle magnetoresistance (HMR), can be present, in addition to SMR, in the observed resistance modulation along the α and β directions as shown in Fig. 2a, b. HMR, typically ascribed to the dephasing of the spin accumulation at the Pt interface, exists in pure Pt independent of adjacent magnetic layer and scales with the applied field strength^{27,28}. In contrast, the SMR requires the presence of an adjacent para-/(Anti)ferro-/ferri-magnetic layer. In order to disentangle the HMR response from SMR, control experiments on a Pt/SiO₂ device, were carried out in order to confirm the observed SMR response in Pt/NGO bilayer (Figs. 4 [d, e]). As is seen in Fig. 4(d), angle dependent magnetoresistance is barely observed in the Pt/SiO₂ device, implying that the observed ADMR response in NGO along in-plane configuration results from SMR effect. This supports the fact that the NGO moments are indeed responsible for the observed ADMR response along the in-plane direction. Also the temperature dependence of ADMR amplitudes obtained for both Pt/NGO and Pt/SiO₂ exhibits distinct temperature dependent behavior, characteristic of SMR and HMR^{27,28} respectively[Fig. 4 (d, e)].

The observation of a small longitudinal-SMR response (i.e. $\Delta R_{xx}/R_o$, as observed in ADMR measurements) and its reduction with temperature (shown in Fig. 2a) can be attributed to a large Drude background

resistivity (resulting from a 11 nm-thick Pt layer) which significantly masks the longitudinal SMR response²⁹. Thus, to minimize the background resistance influence of the Pt layer, we have performed measurements in the transverse configuration (i.e. $\Delta R_{xy}/R_o$). The obtained (ADMR) response in the transverse configuration at 5 K displays a clear $\sin(2\alpha)$ feature, consistent with Eq. 2 (Fig. 4b). Also, the SMR amplitudes acquired by fitting the $\Delta V_{xy}^{1\omega}$ signal to $\sin(2\alpha)$ function scales linearly with the applied current bias implying that the measured ADMR response originates from the SMR effect⁸[Fig. 4c].

Further to the analysis of the obtained data, we consider the role of magnetic anisotropy in such orthorhombic substrates. Orthorhombic substrates such as DyScO₃³⁰, NdGaO₃¹⁸, etc. are known to exhibit magnetic anisotropy at low temperatures along dissimilar crystal axes since anisotropy in magnetic properties or susceptibility can occur generally in any crystalline structure which deviates from the cubic symmetry. This is manifested as differences in the magnetization data acquired along $[001]_o$ and $[-110]_o$ axes in NGO and are the relatively hard and easy axes respectively[Fig. 5(a, b)]. In order to study the impact of magnetic anisotropy on spin transport we have fabricated Pt Hall bars oriented with respect to the in-plane crystalline axes of the NGO substrate (shown in Fig. 5d). This allows us to investigate the SMR response for two different current directions i.e. along the $[-110]_o$ direction and the $[001]_o$ directions of NGO respectively. Such studies can provide useful insights on the role of magnetic anisotropy and Pt/NGO interface quality on spin transport.

From equations 1 and 2, it is evident that any contribution from the magnetic anisotropy will be prominently manifested in the SMR response measured along the longitudinal configuration (longitudinal SMR response is dependent only on the m_y component, i.e. $\Delta R_{xx}/R_o \propto 1 - m_y^2 > \propto \cos^2(\alpha)$). Thus, a larger longitudinal SMR response is expected along the relatively easy axis i.e. $[-110]_o$ compared to $[001]_o$ axis (according to the magnetization data Fig. 5[a, b]). However, we find a finite longitudinal SMR response along $[001]_o$ axis (relatively hard axis) but negligible SMR response along $[-110]_o$ (relatively easy axis) at low temperatures [Fig. 5(c, d)].

On the other hand, the SMR response measured along the transverse direction should be insensitive to the magnetic anisotropy of the underlying magnetic layer according to the eq. 2, since $\Delta R_{xy}/R_o \propto m_x m_y > \propto \sin(2\alpha)$. Thus, the transverse SMR response measured along the orthogonal in-plane axes should yield similar ($\Delta R_{xy}/R_o$) amplitudes, which is contrary to our experimental results along $[-110]_o$ and $[001]_o$ directions [Fig. 5(e, f)]. Such distinct transverse SMR response may be attributed to subtle differences in the NGO surface morphology, either due to substrate steps and terraces, evident in AFM images or to variations in the Pt thickness and morphology, or related to the fabrication of different

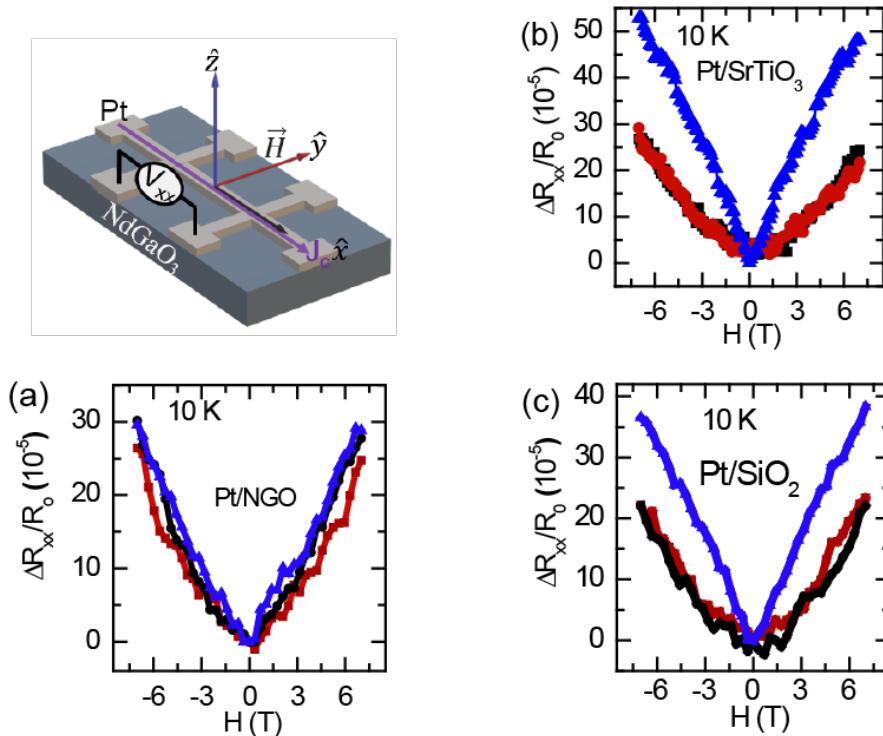


FIG. 3. (a, b, c) Magnetic field dependent magnetoresistance (FDMR) data ($\Delta\rho_{xx}/\rho_0$) obtained along the longitudinal contacts for the three orthogonal crystallographic axes at 10 K, for (a) Pt/NGO, (b) Pt/SrTiO₃ and (c) Pt/SiO₂ devices respectively. The corresponding measurement schematic illustration (black, red, blue curves corresponds to \hat{x} , \hat{y} , \hat{z} directions respectively) employed for acquisition of FDMR.

Pt Hall bars on the orthorhombically distorted-NGO substrate. The observation of different Drude resistivity values of Pt along orthogonal axes [Fig. 5f(inset)] is in line with our argument above and consistent with the previous report³¹.

The minor differences in the transverse SMR results (Fig. 5(e, f)) and Pt resistivity values along $[-110]_o$ and $[001]_o$ directions [Fig. 5f(inset)] can be explained by reduced interface scattering and incremental enhancement in the effective spin conductance³¹. This can facilitate interaction between the 6s spins in the Pt layer and Nd³⁺ 4f orbital spins across the Pt/NGO interface, leading to the observation of a larger transverse SMR amplitude along $[001]_o$ as compared to $[-110]_o$ axis.

Further, we also find that the temperature dependence of the SMR amplitude decreases and vanishes beyond 250 K for the Pt/NGO device at 7 T as shown in Fig. 5(f). This follows the temperature dependence of the magnetization in NGO. The temperature dependence of SMR in NGO and its reduction at high temperatures can be correlated to the increased thermal agitation of the localized spins. This highlights SMR as an effective probe of magnetization in materials that not only exhibit long range ordering but also that arises from localized spins such as in PM.

IV. DISCUSSION

The interaction between the Nd³⁺ moments in paramagnetic NGO is not strong enough to yield the observed SMR signals existing upto high temperatures. In GGG, with weak spin orbit interaction, the observed spin transport was explained in terms of dipolar exchange interactions¹² or short-range correlations²⁰ whereas in another paramagnet, Tb₃Ga₅O₁₂, with a finite orbital angular moment ($L=3$), the authors do not observe any such signatures. They highlight the importance of the weak spin-lattice coupling in long-range paramagnetic spin transmission in GGG. In NGO with $L=6$, a strong correlation between spin and orbital angular momentum is expected, however we do observe clear signatures of SMR. To understand the underlying mechanism, we propose the role of temperature driven electronic excitations between the crystal field split levels (ground $[4I_{9/2}]$ and excited states $[4I_{11/2}]$) in Nd³⁺. In related studies on neutron diffraction in NGO²³, the authors unambiguously ascertain four inelastic peaks of magnetic origin and show

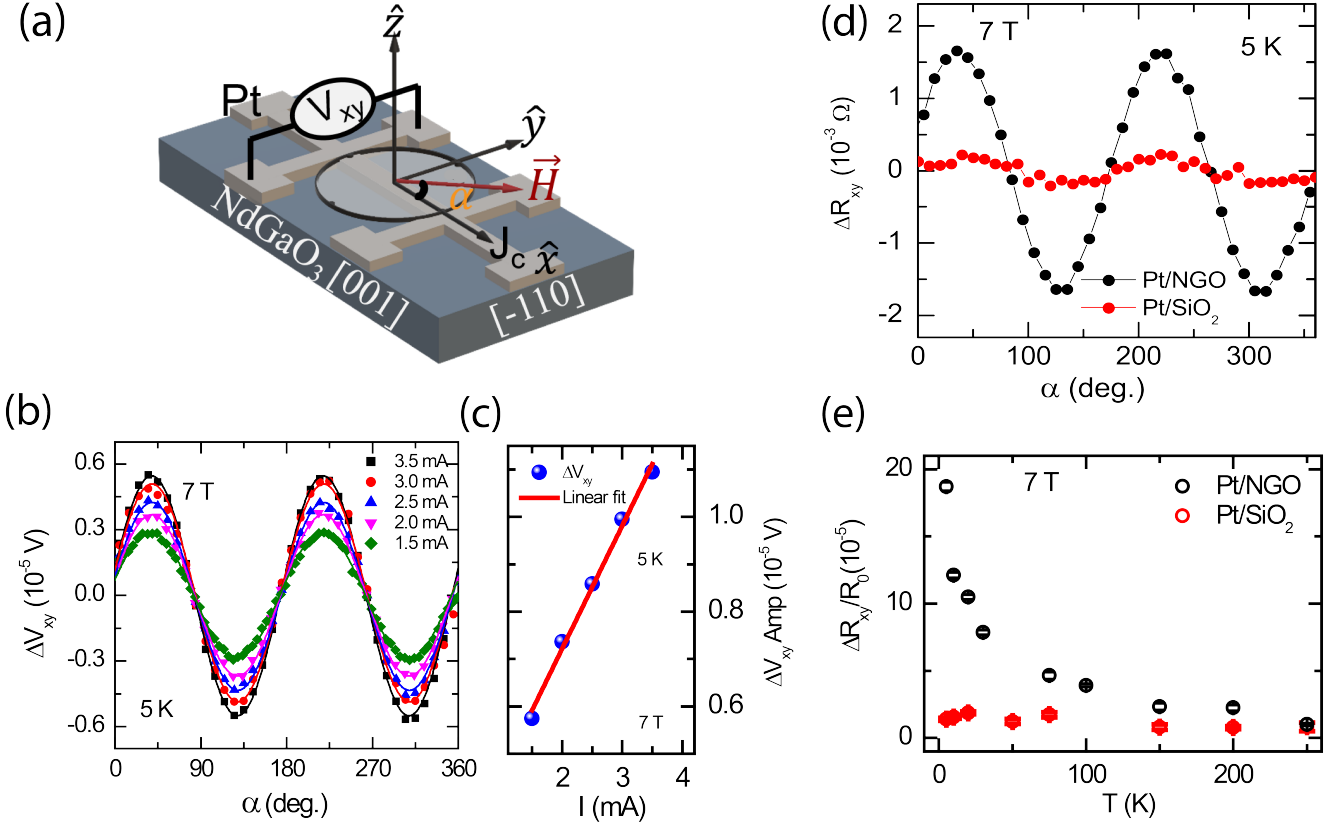


FIG. 4. (a) Schematic illustration of the Hall bar geometry employed for observation of transverse-SMR response across (11nm) Pt /NdGaO₃ (110)o. (b) Angular dependent magnetoresistance (ADMR) signals (V_{xy}) are shown for different current bias, and by rotating the sample in the plane of the transport (x-y plane) at a constant magnetic field of 7 T. (c) shows the linear current dependence of ΔV_{xy} amplitude obtained from the $\sin^2(\alpha)$ function fits (solid lines) to experimental data (ΔV_{xy}) at 5 K. (d) shows the comparison of ADMR signals obtained for Pt/NGO and Pt/SiO₂ samples acquired for lowest possible temperature 5 K and high magnetic field of 7 T in our system in order to observe any SMR signals for Pt/SiO₂. As one could infer even for 5 K and 7 T field, Pt/SiO₂ sample exhibits negligible ADMR response in comparison to Pt/NGO, (e) shows the temperature dependence of ADMR amplitudes obtained for Pt/NGO and Pt/SiO₂ samples at 7 T field which clearly depicts two distinct behaviors i.e. SMR response in Pt/NGO and characteristic HMR response (as described in the text) in Pt/SiO₂.

that the ten-fold degeneracy of the ground-state [$4I_{9/2}$] of the Nd³⁺ ions is split by the crystalline electric field (CEF) into five Kramers doublet levels. At temperatures between 12-150 K, the thermal energy ($k_B T$) drives the transitions between these doublet ground state [$4I_{9/2}$] levels with the energy spectra lying between 11 and 70 meV. Further increasing temperature (beyond 150 K) leads to the additional electronic excitations/transitions between the excited states [$4I_{11/2}$] in Nd³⁺. This sets in self-interaction between 4f orbitals in NGO, leading to ordering of localized moments.

We also consider interfacial spin flip scattering¹² induced spin excitations between the Zeeman split levels (i.e. $g_j \Delta m_j \mu_B B$, $\Delta m_j = \pm 1$ represents the possible allowed transitions, here g_j is Lande g factor, m_j is magnetic quantum number, μ_B is the Bohr magneton). In presence of an external magnetic field, the degeneracy of Nd³⁺ localized 4f orbitals is lifted further, leading to different

energy levels (as shown in Fig. S3a) where the energy spacing (i.e. $g_j \Delta m_j \mu_B B$) scales with the external field strength. At Pt/NGO interface, the spin interaction between Pt (6s) conduction electrons with Nd³⁺ localized spins alters the spin state by an energy of $g_j \Delta m_j \mu_B B$ leading to a non-equilibrium state (Fig. S3b) of localized spins. This results in a gradient of the spin chemical potential (μ_{PI}) and a spin current diffusion that is proportional to the difference in spin chemical potential μ_{PI} and electronic chemical potential μ_{HM} , across the interface¹² as follows:

$$J_s = \left(\frac{h}{2\pi e^2}\right) g_s (\mu_{PI} - \mu_{HM}) \quad (3)$$

Here g_s is the effective spin conductance which governs the coupling between the spin chemical potential and the spin accumulation across the Pt/NGO interface.

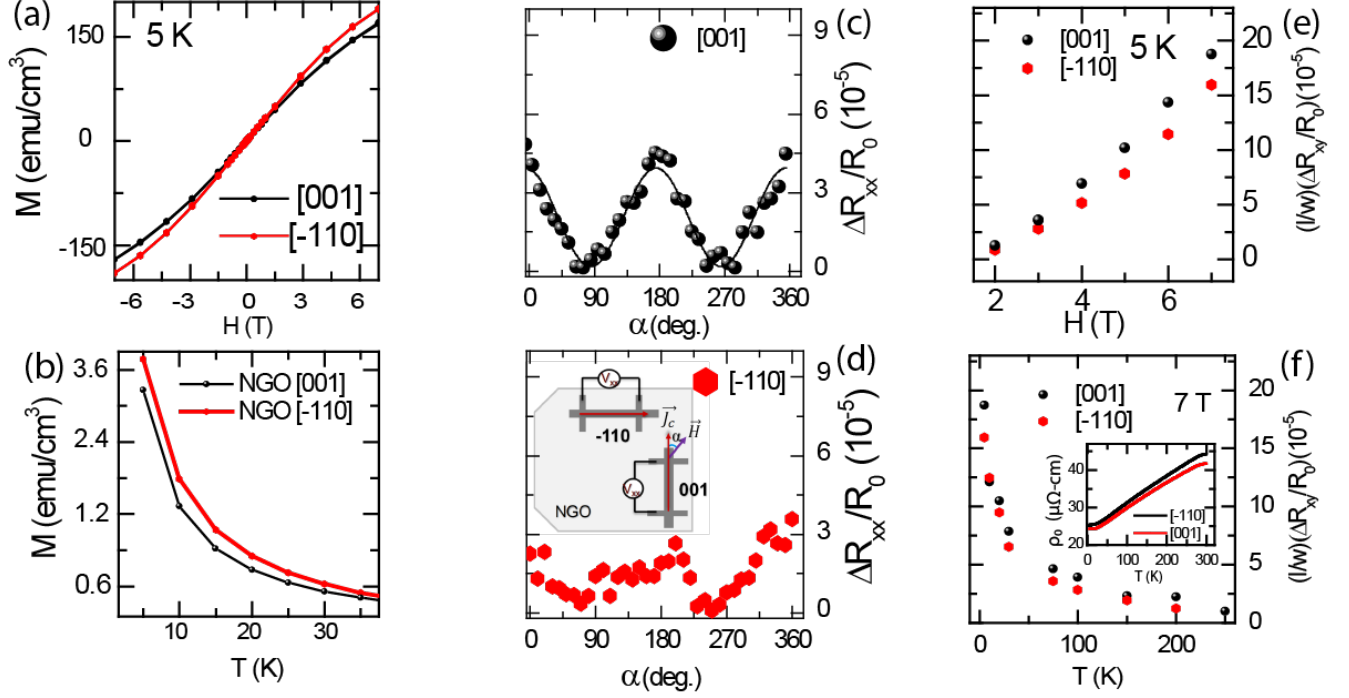


FIG. 5. (a, b) Magnetization (M) vs applied magnetic field (H), and M vs temperature (T) plotted along two in-plane orthogonal (i.e. $[001]_o$ and $[-110]_o$) crystallographic axes. (c, d) Angular dependent spin Hall magnetoresistance (ADMAR) signals ($\Delta R_{xx}/R_0$) measured along the longitudinal contacts across (11 nm) Pt /NdGaO₃ (110)_o sample by rotating the sample in-plane at a constant field of 7 T, and by applying the current bias along (001) and (-110) directions respectively (solid line is a fit to SMR data following eq. 1). (e, f) depicts the magnetic field and temperature dependence of $(\frac{l}{w})(\frac{\Delta R_{xx}}{R_0})$ amplitudes respectively along two in-plane axes (here l, w are length, width of longitudinal contacts as per eq. 1). Inset to 5 (f) depicts the corresponding temperature dependent longitudinal Drude resistivity of Pt along the two in-plane axes.

V. CONCLUSION

Thus we conclude that the magnetic properties in perovskite paramagnetic NGO, that leads to the observation of SMR upto 250 K has its origin in the self-interactions between the correlated 4f orbitals due to crystal field effects, J mixing between the multiplets and the temperature driven electronic excitations between crystal field split levels. Our angle dependent-MR measurements reveal spin dependent magnetoresistance modulation effect in paramagnetic NGO persisting beyond T_N in a temperature regime much higher than reported for paramagnetic GGG. Control experiments on Pt/SiO₂ sample were also carried out in order to substantiate the observed SMR response in Pt/NGO bilayer and decouple the role of possible intrinsic effects in Pt due to HMR/WAL. Low temperature SMR studies (spanning across the NGO magnetic phase transition) will be interesting to understand the impact of AFM exchange interaction on the SMR response. Our work also underpins the need for new considerations to the theoretical framework of

SMR in encompassing diverse materials beyond those that order spontaneously and which exhibit non-zero correlation between spin and orbital angular momentum.

VI. DATA AVAILABILITY

The data that support the findings of this study are available from the corresponding author upon reasonable request.

VII. ACKNOWLEDGEMENTS

The authors thank A. S. Goossens, Jacob Baas, J.G. Holstein, H.H. de Vries, T. J. Schouten for technical support. This work is realized using the facilities available at NanoLab NL and is supported by the Dieptestrategie grant from the Zernike Institute for Advanced Materials, University of Groningen. V.E.P thanks financial support

from the Spinoza Prize awarded to B. J. van Wees by NWO.

-
- * corresponding author; e.p.vallabhaneni@rug.nl
 † corresponding author; t.banerjee@rug.nl
- ¹ Y. T. Chen, S. Takahashi, H. Nakayama, M. Althammer, S. T. Goennenwein, E. Saitoh, and G. E. Bauer, *Physical Review B* **87**, 144411 (2013).
 - ² Y. T. Chen, S. Takahashi, H. Nakayama, M. Althammer, S. T. Goennenwein, E. Saitoh, and G. E. Bauer, *Journal of Physics Condensed Matter* **28**, 103004 (2016).
 - ³ M. Althammer, S. Meyer, H. Nakayama, M. Schreier, S. Altmannshofer, M. Weiler, H. Huebl, S. Geprags, M. Opel, R. Gross, D. Meier, C. Klewe, T. Kuschel, J. M. Schmalhorst, G. Reiss, L. Shen, A. Gupta, Y. T. Chen, G. E. Bauer, E. Saitoh, and S. T. Goennenwein, *Physical Review B* **87**, 224401 (2013).
 - ⁴ H. Nakayama, M. Althammer, Y. T. Chen, K. Uchida, Y. Kajiwara, D. Kikuchi, T. Ohtani, S. Geprags, M. Opel, S. Takahashi, R. Gross, G. E. Bauer, S. T. Goennenwein, and E. Saitoh, *Physical Review Letters* **110**, 206601 (2013).
 - ⁵ N. Vlietstra, J. Shan, V. Castel, B. J. Van Wees, and J. Ben Youssef, *Physical Review B* **87**, 184421 (2013).
 - ⁶ M. Isasa, S. Velez, E. Sagasta, A. Bedoya-Pinto, N. Dix, F. Sanchez, L. E. Hueso, J. Fontcuberta, and F. Casanova, *Physical Review Applied* **6**, 034007 (2016).
 - ⁷ G. R. Hoogeboom, A. Aqeel, T. Kuschel, T. T. Palstra, and B. J. Van Wees, *Applied Physics Letters* **111**, 052409 (2017).
 - ⁸ J. Fischer, O. Gomonay, R. Schlitz, K. Ganzhorn, N. Vlietstra, M. Althammer, H. Huebl, M. Opel, R. Gross, S. T. Goennenwein, and S. Geprags, *Physical Review B* **97**, 014417 (2018).
 - ⁹ L. Baldrati, A. Ross, T. Niizeki, C. Schneider, R. Ramos, J. Cramer, O. Gomonay, M. Filianina, T. Savchenko, D. Heinze, A. Kleibert, E. Saitoh, J. Sinova, and M. Klaui, *Physical Review B* **98**, 024422 (2018).
 - ¹⁰ R. Lebrun, A. Ross, O. Gomonay, S. A. Bender, L. Baldrati, F. Kronast, A. Qaiumzadeh, J. Sinova, A. Brataas, R. A. Duine, and M. Klaui, *Communications Physics* **2**, 50 (2019).
 - ¹¹ A. Das, V. E. Phanindra, A. J. Watson and T. Banerjee, *Appl. Phys. Lett* **118**, 052407 (2021).
 - ¹² K. Oyanagi, S. Takahashi, L. J. Cornelissen, J. Shan, S. Daimon, T. Kikkawa, G. E. Bauer, B. J. van Wees, and E. Saitoh, *Nature Communications* **10**, 062030 (2019).
 - ¹³ L. Liang, J. Shan, Q. H. Chen, J. M. Lu, G. R. Blake, T. T. Palstra, G. E. Bauer, B. J. Van Wees, and J. T. Ye, *Physical Review B* **98**, 134402 (2018).
 - ¹⁴ K. Oyanagi, J. M. Gomez-Perez, X. P. Zhang, T. Kikkawa, Y. Chen, E. Sagasta, L. E. Hueso, V. N. Golovach, F. S. Bergeret, F. Casanova, and E. Saitoh, arXiv:2008.02446 (2020).
 - ¹⁵ M. Lammel, R. Schlitz, K. Geishendorf, D. Makarov, T. Kosub, S. Fabretti, H. Reichlova, R. Huebner, K. Nielsch, A. Thomas, and S. T. Goennenwein, *Applied Physics Letters* **114**, 252402 (2019).
 - ¹⁶ S. S. Parkin, N. More, and K. P. Roche, *Physical Review Letters* **64**, 2304 (1990).
 - ¹⁷ X. P. Zhang, F. S. Bergeret, and V. N. Golovach, *Nano Letters* **19**, 6330 (2019).
 - ¹⁸ F. Luis, M. Kuz'min, F. Bartolome, V. Orera, J. Bartolome, M. Artigas, and J. Rubın, *Physical Review B* **58**, 798 (1998).
 - ¹⁹ H. Boschker, M. Mathews, E. P. Houwman, H. Nishikawa, A. Vailionis, G. Koster, G. Rijnders, and D. H. Blank, *Physical Review B* **79**, 214425 (2009).
 - ²⁰ S. M. Wu, J. E. Pearson, and A. Bhattacharya, *Physical Review Letters* **114**, 186602 (2015).
 - ²¹ Y. Yamamoto, M. Ichioka, and H. Adachi, *Physical Review B* **100**, 064419 (2019).
 - ²² W. Marti, P. Fischer, J. Schefer, and F. Kubel, *Z. Kristallogr.* **211**, 891 (1996).
 - ²³ A. Podlesnyak, S. Rosenkranz, F. Fauth, W. Marti, A. Furrer, A. Mirmelstein, and H. J. Scheel, *Journal of Physics: Condensed Matter* **5**, 8973 (1993).
 - ²⁴ P. Novak, K. Knizek, M. Marysko, Z. Jirak, and J. Kunes, *Journal of Physics: Condensed Matter* **25**, 446001 (2013).
 - ²⁵ B. K. De, V. Dwij, M. K. Gupta, R. Mittal, H. Bhatt, V. R. Reddy, and V. G. Sathe, *Physical Review B* **103**, 054106 (2021).
 - ²⁶ K. Steenbeck, T. Habisreuther, and R. Mattheis, *Journal of Applied Physics* **109**, 073906 (2011).
 - ²⁷ S. Velez, V. N. Golovach, A. Bedoya-Pinto, M. Isasa, E. Sagasta, M. Abadia, C. Rogero, L. E. Hueso, F. S. Bergeret, and F. Casanova, *Physical Review Letters* **116**, 016603 (2016).
 - ²⁸ H. Wu, X. Zhang, C. H. Wan, B. S. Tao, L. Huang, W. J. Kong, and X. F. Han, *Physical Review B* **94**, 174407 (2016).
 - ²⁹ A. Aqeel, N. Vlietstra, J. A. Heuver, G. E. Bauer, B. Noheda, B. J. Van Wees, and T. T. Palstra, *Physical Review B* **92**, 224410 (2015).
 - ³⁰ X. Ke, C. Adamo, D. G. Schlom, M. Bernhagen, R. Uecker, and P. Schiffer, *Applied Physics Letters* **94**, 152503 (2009).
 - ³¹ M. Althammer, A. V. Singh, T. Wimmer, Z. Galazka, H. Huebl, M. Opel, R. Gross, and A. Gupta, *Applied Physics Letters* **115**, 092403 (2019).